Diabatic Eddy Forcing Increases Persistence and Opposes Propagation of the Southern Annular Mode in MERRA2

Supplemental Materials

Samuel Smith[1,2]*, Jian Lu[3], Paul W. Staten[2]

[1]University of Chicago, Chicago, IL

[2]Indiana University, Bloomington, IN

[3]Pacific Northwest National Laboratory, Richland, WA

*Contact information: samuelsmith@uchicago.edu

Scaling of Diabatic FAWA Source

Beginning with the definition of the vertically-integrated diabatic heat source (c.f. Eq. (5) in the main text), using the alternative but equivalent definition of the FAWA integral (see Huang and Nakamura 2016)

$$\Delta\Sigma \equiv -\frac{a}{2\pi\cos\phi_e}\int_{p_b}^{p_t}\int_0^{2\pi}\int_0^{\Delta\phi} f\frac{\partial}{\partial p}\left(\frac{\dot{\theta}_d}{d\widetilde{\theta}/dp}\right)\cos\phi\, d\lambda d\phi' dp. \tag{S1}$$

Here we introduce $\dot{\theta}_d \equiv (p_R p^{-1})^{\kappa} c_p^{-1} J_T$ which is the potential temperature tendency due to diabatic heat release. As in Huang and Nakamura (2016, hereafter HN16), ϕ' coordinates are a variable of integration between the equivalent latitude ϕ_e and the Q contour. $\Delta\phi(\lambda,\phi,\phi',p)$ can be multivalued, e.g., in the case of a cutoff low. See HN16 for more details.

We aim to simplify (S1) to build a physical intuition for how diabatic heating interacts with the mean flow in the FAWA framework. We make a series of assumptions to do this; these assumptions are not expected to provide accurate numerical computation of Eq. (S1), as numerical computation is done using Eq. (5). Rather, we only aim for a scaling which follows the general form of Eq. (S1).

First, we assume that the upper-level waves are relatively barotropic such that $\Delta\phi$ has relatively weak dependence on height, so that we can move the vertical integral in Eq. (S1) to the innermost position and eliminate it using the fundamental theorem of calculus

$$\Delta\Sigma \sim -\frac{a}{2\pi\cos\phi_e}\int_0^{2\pi}\int_0^{\Delta\phi} f\left(\frac{\dot{\theta}_d}{d\tilde{\theta}/dp}\right)_{p_b}^{p_t}\cos\phi\, d\lambda d\phi'. \tag{S2}$$

Next, we make use of the relationship that FAWA scales as $A \sim a\Delta\phi(q-Q) \equiv \eta q_e$ (see Nakamura and Zhu 2010, HN16, and Smith et al. 2021), where η is the cartesian length of the Q contour displacement, proportional to the meridional eddy stirring scale, and q_e is an eddy PV anomaly (the integrand in the FAWA calculation). In the same vein, we assume the innermost integral in Eq. (S2) should scale similarly, with the ratio $\frac{\cos\phi}{\cos\phi_e}\sim 1$

$$\Delta\Sigma \sim -\frac{1}{2\pi}\int_0^{2\pi}\eta f\left(\frac{\dot{\theta}'_d}{d\tilde{\theta}/dp}\right)_{p_b}^{p_t} d\lambda \tag{S3}$$

Note here the introduction of the prime on $\dot{\theta}_d$ to indicate the heating is an eddy term similar to q_e. Finally, we contend that $\dot{\theta}'_d \sim \Delta\theta'_d(\tau)^{-1}$, where $\Delta\theta'_d$ is the diabatic adjustment to potential temperature within an eddy during its lifetime, and τ is the eddy lifetime. Thus, we can approximate $\eta\tau^{-1}\sim v'_\tau$ as a kind of meridional transport velocity by midlatitude eddies, enabling a final simplification of Eq. (S3)

$$\Delta\Sigma \sim -f\left(\frac{\overline{v'_\tau\Delta\theta'_d}}{d\tilde{\theta}/dp}\right)_{p_b}^{p_t} \tag{S4}$$

Compare Eq. (S4) to the baroclinic term in Eq. (6) in the main text

$$-f\left(\frac{\overline{v'_g\theta'}}{d\tilde{\theta}/dp}\right)\Bigg|_{500}.$$

Thus, Eq. (S4) suggests that diabatic heating injects momentum into the mean flow in a similar process to the baroclinic injection performed by the vertical component of the Eliassen-Palm flux.

Moreover, Eq. (S3) can be utilized to estimate an expected magnitude for the diabatic wave source, using $\eta = 100km; f = 1 \times 10^{-4}\ s^{-1}; \theta_d = 10K\ day^{-1}; d\tilde{\theta}/dp\ = 0.1K\ hPa^{-1}$:

$$\Delta\Sigma \sim \frac{f\eta'\dot{\theta_d}'}{500\ hPa \cdot d\tilde{\theta}/dp} \sim 2\ m/s/day,$$

which is close to the hemispheric-mean value seen in Figure S1.

Supplemental Figures

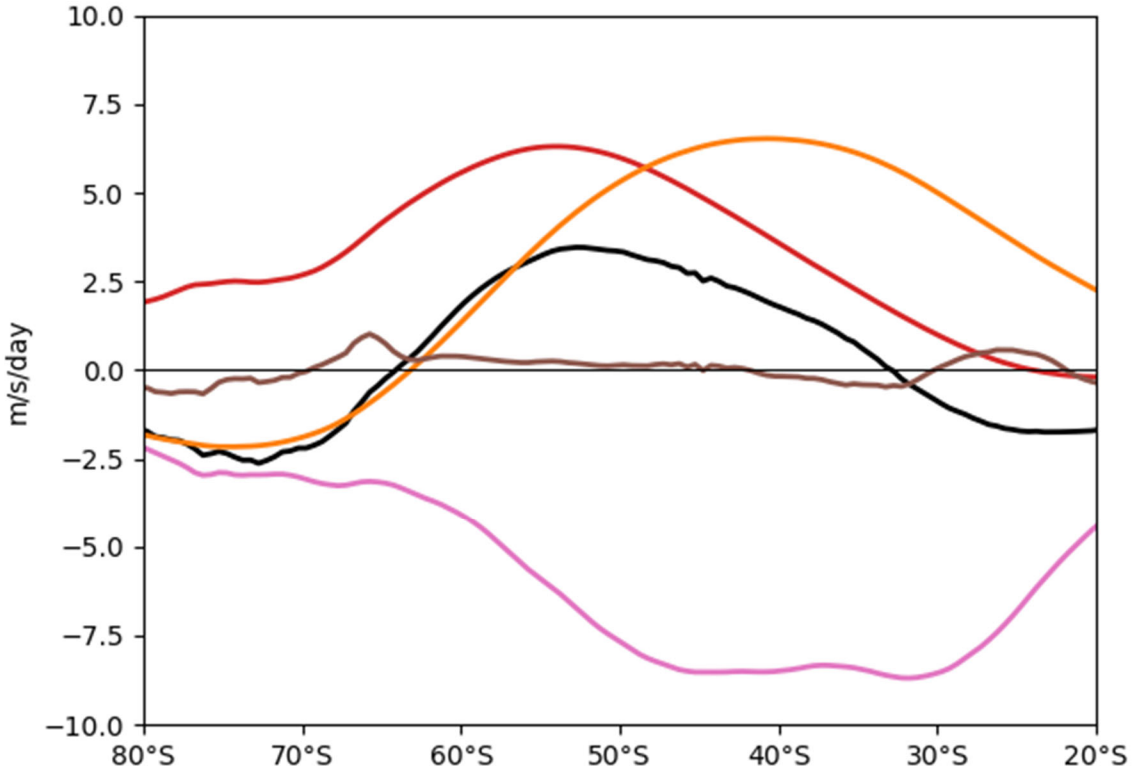

Figure S1: The climatological-mean partitioning of EMFC using the FAWA budget from MERRA2 data, 2005-2019. See Eq. 8 for more details.

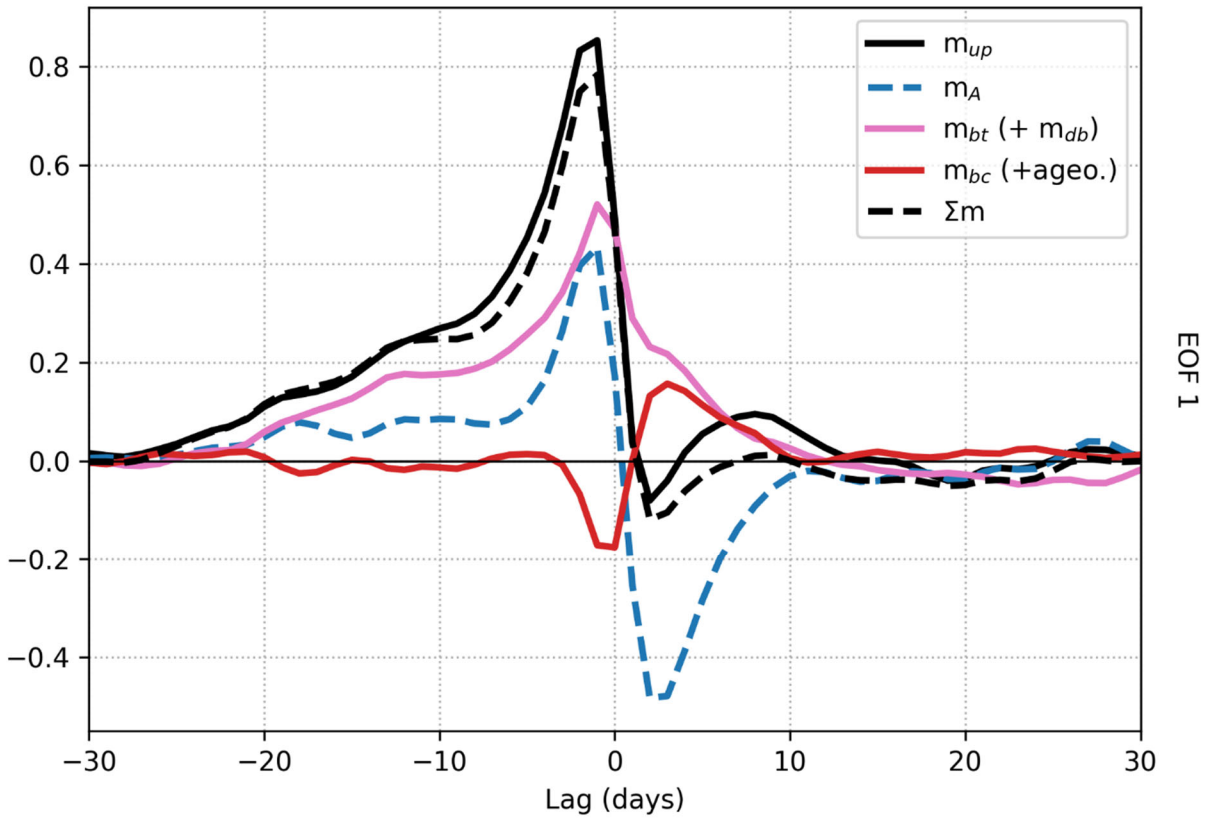

Figure S2: As in Figure 2, but in the style of Nie et al. (2014; see their Figure 2a)'s budget of the eddy momentum flux convergence, produced using the year-round MERRA2 data from 2005-2019 used for this study, only for EOF1. To match the magnitudes obtained by Nie et al. (2014), we down-sample the 6-hourly data to daily, while also coarsening the latitudinal resolution from 0.5° to 2.5° since the magnitude of a linear projection is sensitive to the horizontal resolution (see section 4.1). The PC index is taken to vary from -1 to 1 instead of having unit variance. Finally, we combine $m_{db} + m_{bt}$ for m_{bt} and take the full eddy heat flux rather than just the geostrophic for m_{bc} (see section 2.1).

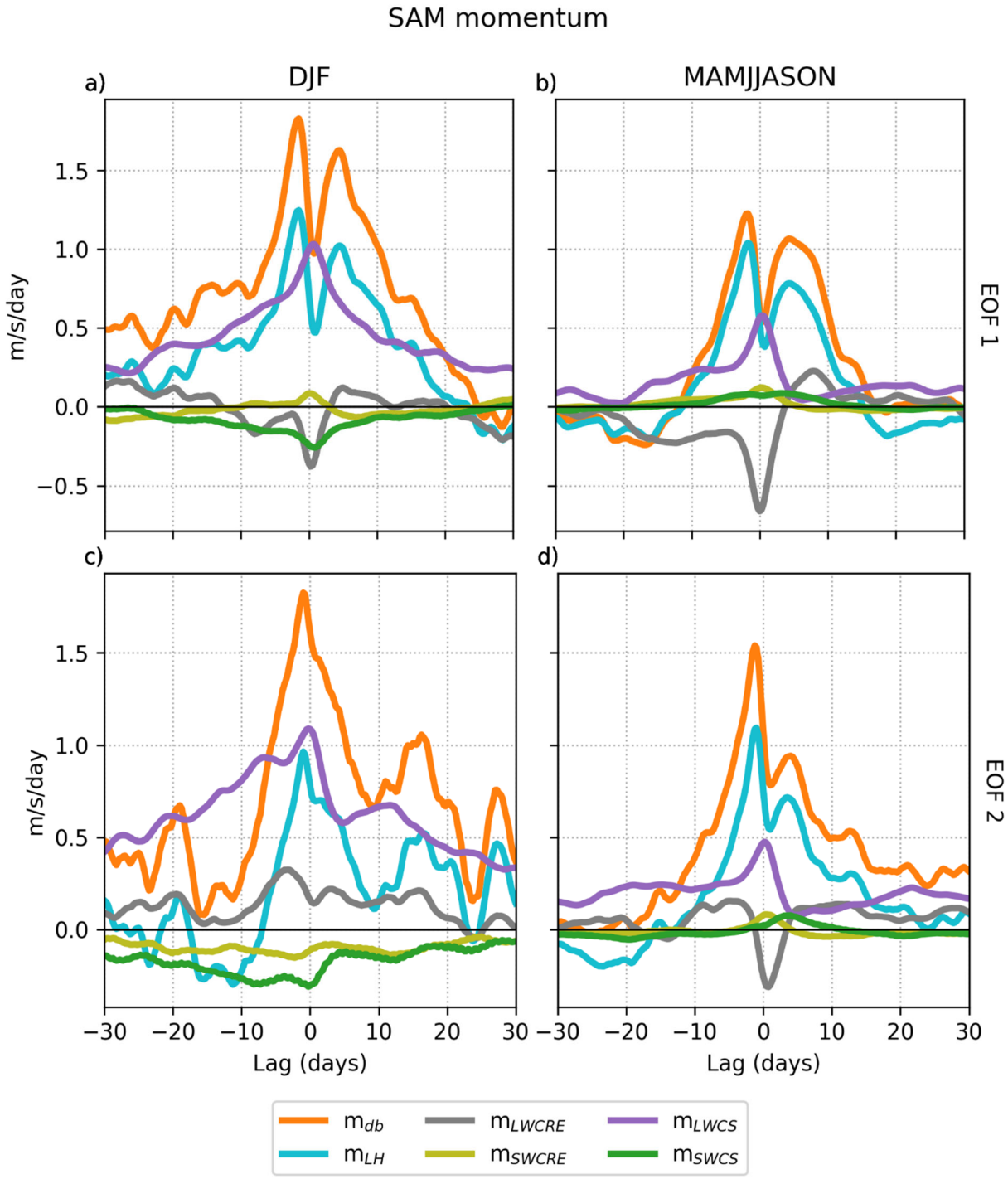

Figure S3: As in Figure 5, but including shortwave cloud (m_{SWCRE}) and clear-sky (m_{SWCS}) contributions, which are included in the total (m_{db}). Decompositions into cyclonic and anticyclonic contributions are not shown.

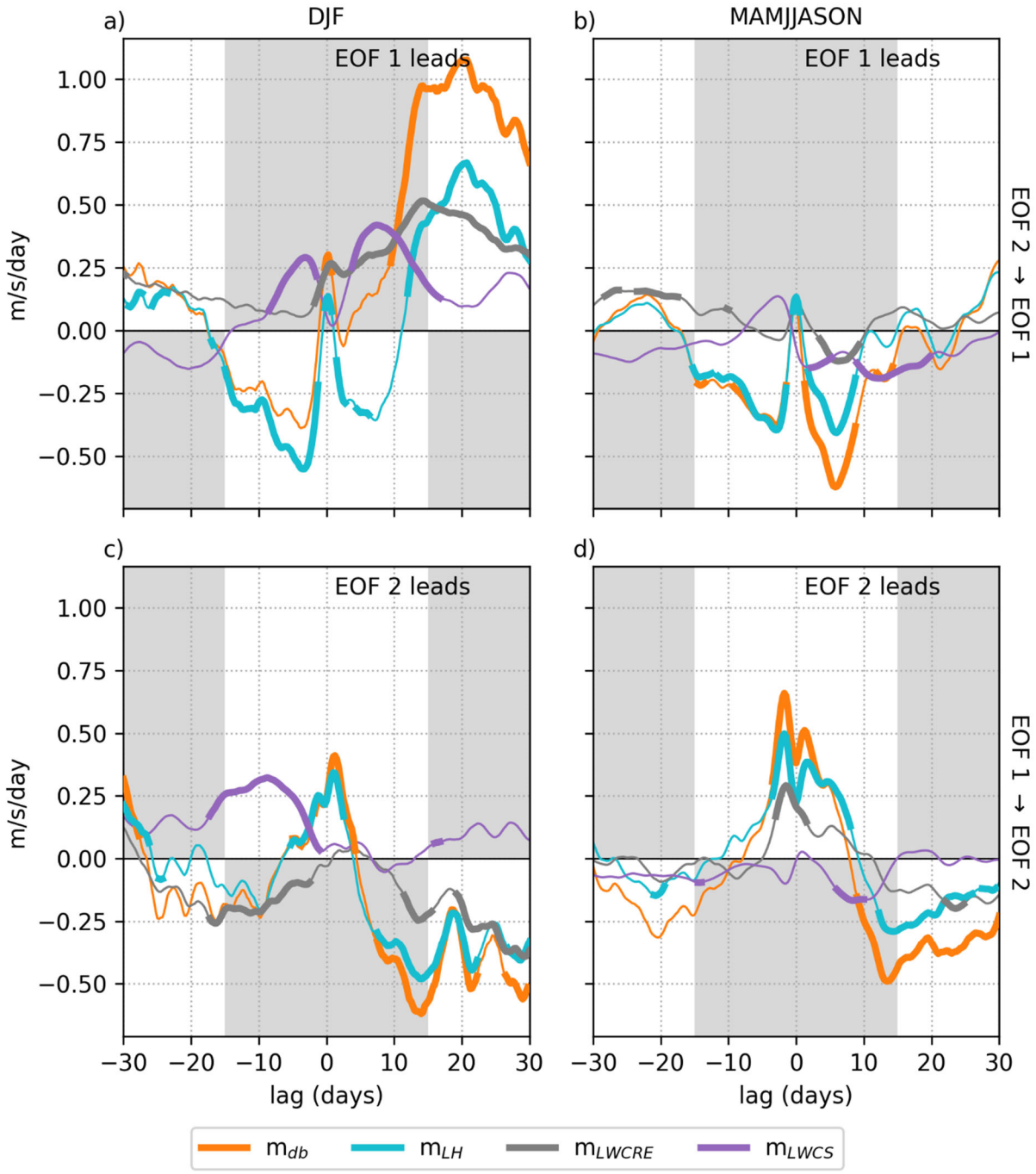

Figure S4: As in Figure 3a-d, but for each diabatic process separately (as in Figure 5).

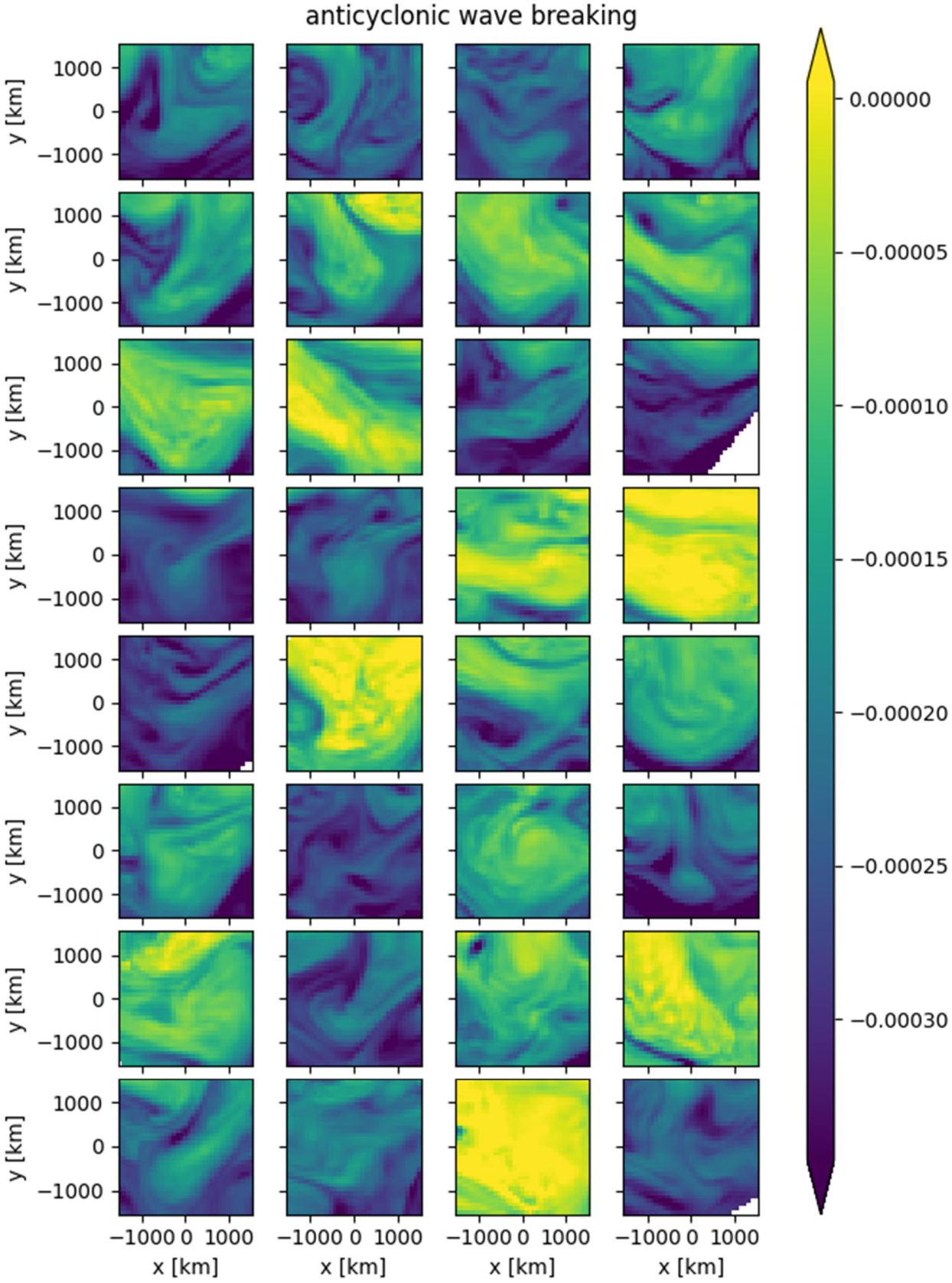
anticyclonic wave breaking
y [km]
1000
0
−1000
x [km]
−1000 0 1000
0.00000
−0.00005
−0.00010
−0.00015
−0.00020
−0.00025
−0.00030

Figure S5: A random sample of anticyclonic wave breaking events identified by the wave activity tracking procedure described in section 3.2 for MERRA2 from 2005-2019. Shading is quasi-geostrophic potential vorticity taken at the same time and with the same central latitude/longitude as identified in the wave activity field. The x-coordinate is positive eastward, and the y-coordinate is positive northward. Missing values result when the data is too close to the pole to be properly interpolated.

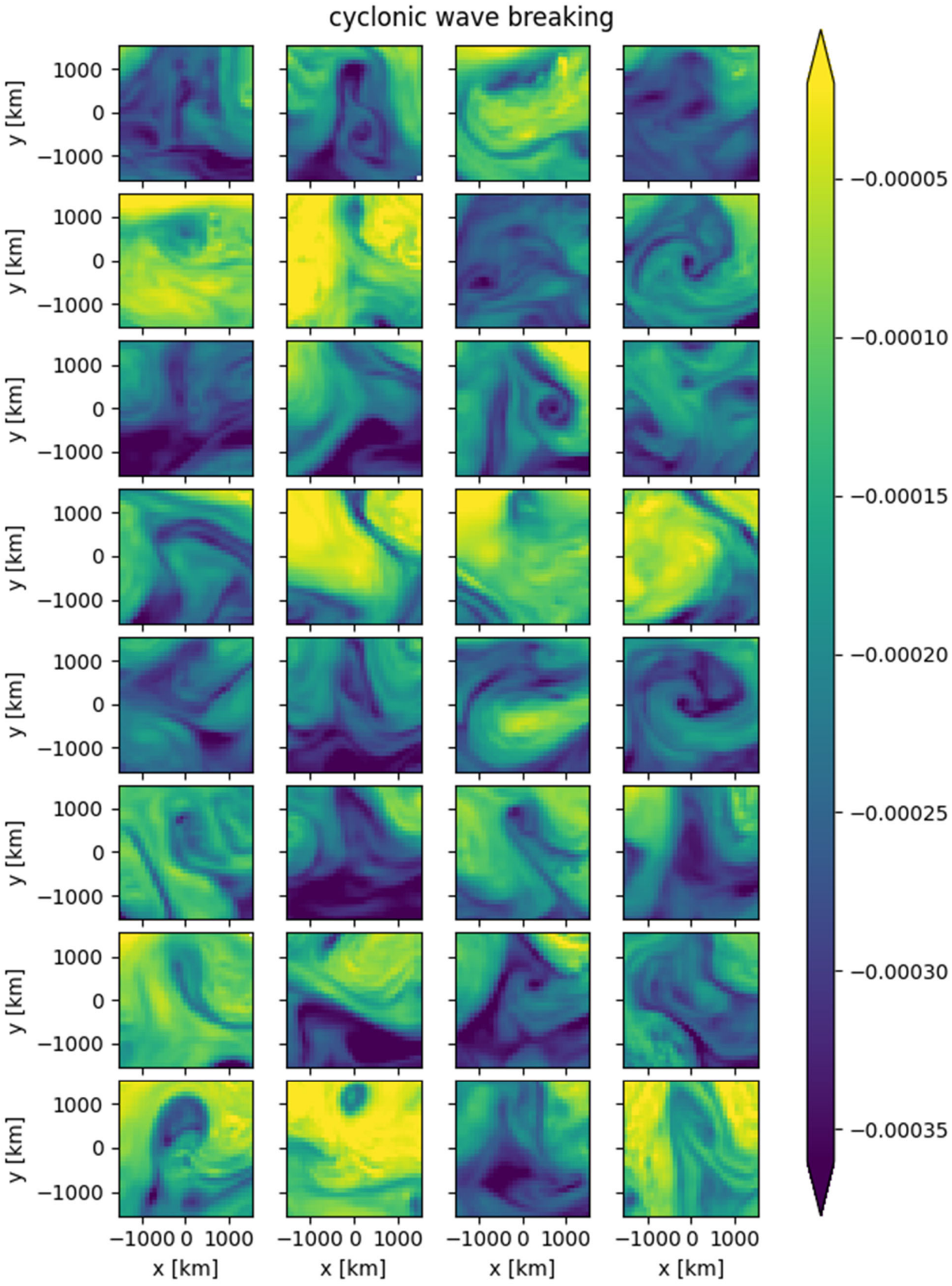

Figure S6: As in Figure S3, but for cyclonic wave breaking events.

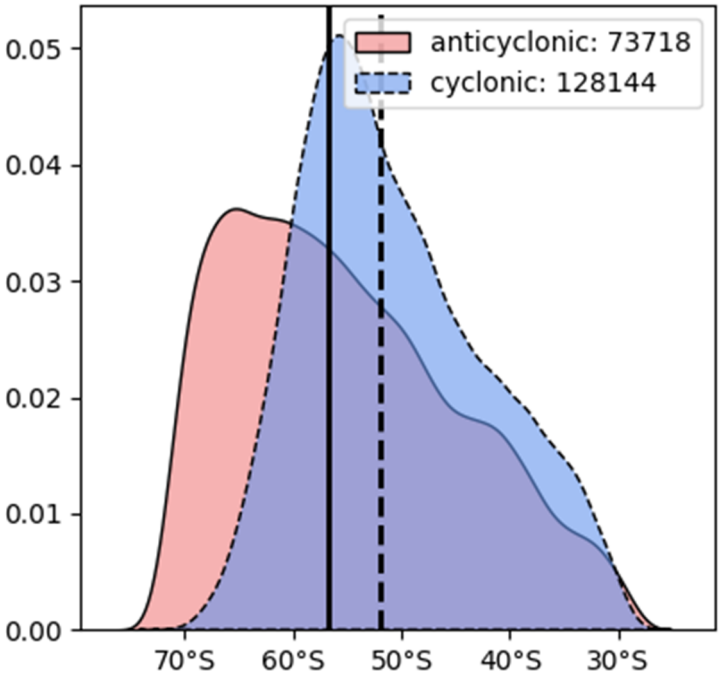

Figure S7: Probability distribution functions (PDFs) showing the counts and distribution of cyclone and anticyclone central latitudes in MERRA2 (2005-2019) identified using the method outlined in section 3.2. Distributions are year-round and for cyclones/anticyclones used in the 10-day lagged analysis of section 4.3. Black vertical lines represent the medians for the anticyclonic (solid) and cyclonic (dashed) waves. Note that latitudes are technically equivalent latitudes (c.f. Huang and Nakamura, 2016).